Eur Radiol (2008) 18: 2174–2181
DOI 10.1007/s00330-008-0978-x

EXPERIMENTAL

Zhan-Long Ma
Gao-Jun Teng
Jun Chen
Hong-Ying Zhang
Ai-Hong Cao
Yicheng Ni

A rabbit model of atherosclerosis at carotid artery: MRI visualization and histopathological characterization

Received: 20 December 2007
Revised: 6 February 2008
Accepted: 13 March 2008
Published online: 17 April 2008

Z.-L. Ma · G.-J. Teng (✉) · J. Chen · H.-Y. Zhang · A.-H. Cao
Molecular Imaging Laboratory,
Department of Radiology,
Zhong-Da Hospital,
Southeast University,
87# Dingjiaqiao Road,
Nanjing 210009, China
e-mail: gjteng@vip.sina.com
Tel.: +86-25-83272121
Fax: +86-25-83311083

Y. Ni
Department of Radiology,
University Hospitals,
Catholic University of Leuven,
Leuven, Belgium

Abstract To induce a rabbit model of atherosclerosis at carotid artery, to visualize the lesion evolution with magnetic resonance imaging (MRI), and to characterize the lesion types by histopathology. Atherosclerosis at the right common carotid artery (RCCA) was induced in 23 rabbits by high-lipid diet following balloon catheter injury to the endothelium. The rabbits were examined in vivo with a 1.5-T MRI and randomly divided into three groups of 6 weeks (n=6), 12 weeks (n=8) and 15 weeks (n=9) for post-mortem histopathology. The lesions on both MRI and histology were categorized according to the American Heart Association (AHA) classifications of atherosclerosis. Type I and type II of atherosclerotic changes were detected at week 6, i.e., nearly normal signal intensity (SI) of the injured RCCA wall without stenosis on MRI, but with subendothelial inflammatory infiltration and proliferation of smooth muscle cells on histopathology. At week 12, 75.0% and 62.5% of type III changes were encountered on MRI and histopathology respectively with thicker injured RCCA wall of increased SI on T_1-weighted and proton density (PD)-weighted MRI and microscopically a higher degree of plaque formation. At week 15, carotid atherosclerosis became more advanced, i.e., type IV and type V in 55.6% and 22.2% of the lesions with MRI and 55.6% and 33.3% of the lesions with histopathology, respectively. Statistical analysis revealed a significant agreement ($p<0.05$) between the MRI and histological findings for lesion classification ($r=0.96$). A rabbit model of carotid artery atherosclerosis has been successfully induced and noninvasively visualized. The atherosclerotic plaque formation evolved from type I to type V with time, which could be monitored with 1.5-T MRI and confirmed with histomorphology. This experimental setting can be applied in preclinical research on atherosclerosis.

Keywords Atherosclerosis · Magnetic resonance imaging · Carotid artery · Rabbit · Histology

Introduction

Atherosclerosis, the leading cause of mortality and morbidity in the modern societies, is a disease of the vessel wall that occurs in the coronary arteries, carotid arteries, aortas and other peripheral arteries [1, 2]. Convincing evidence has emerged over recent years to support the theory that "endothelial injury" is the initiation of the arteriosclerosis process. Under normal conditions, the endothelium regulates vascular homeostasis through a variety of factors including nitric oxide (NO), prostacyclin and endothelin, which act locally in the vascular wall and lumen. Endothelial dysfunction contributes to enhanced vasoconstrictor responses, adhesion of platelets and monocytes, and proliferation and migration of vascular smooth muscle cells, all of which are the events occurring in atherosclerosis

rosis [3, 4]. Although magnetic resonance imaging (MRI) has already demonstrated its capabilities to identify the anatomy and even pathology of atherosclerotic plaques both in animal models and in human patients, quantification and classification of natural progression of atherosclerosis require a MRI machine with very high spatial resolution [5–8]. On the other hand, an appropriate animal model proves critical to research and development of new diagnostic and therapeutic modalities for conquering a disease. Furthermore, accurate visualization of carotid artery atherosclerosis formation in a small animal model remains a technical challenge. In order to introduce an experimental platform based on our current clinical environment, we have made a series of efforts to induce a model of carotid artery atherosclerosis in rabbits, to visualize the lesion evolution with a clinical 1.5-T MRI system and to characterize lesion types by histopathology. In this technical report, we describe how rabbit carotid artery was injured to trigger plaque formation through a subsequent high-lipid diet and what types of atherosclerosis could be induced as characterized by both MRI and histopathology according to the current standard clinical classifications. We believe that, instead of grouped sacrifice at multiple time points, such an experimental platform would be particularly useful for performing longitudinal follow-up studies on atherosclerosis formation, diagnosis and therapies in the same animals for improved accuracy and efficacy.

Materials and methods

Animal model

This experimental protocol was approved by our institutional committee for animal use and care. A total of 23 male New Zealand white rabbits (Jinlin Farm Inco, Nanjing, China), 3 months of age and 2.0–2.5 kg of body weight, were recruited, fed with high cholesterol diet for 1 week, and then subjected to balloon-induced intimal injury of the right common carotid artery (RCCA). The balloon injury of the RCCA was performed via an interventional approach under a C-arm angiography unit (Innova 3100, GE Medical System). After anesthesia by intravenous injection of 40 mg/kg pentobarbital (Shanghai Chemical Reagent Co., Shanghai), aortic arteriography on bilateral carotid arteries was performed through transcatherization of the right femoral artery with a cut-down technique. A balloon with a diameter of 2.5 mm and a length of 20 mm (Medtronic, AVE, Santa Rosa, CA) was inserted into the RCCA and inflated and deflated three times for 180 s. Carotid arteriography was taken again immediately after transcatheter intervention (Fig. 1). After balloon injury on the RCCA, the rabbit was kept with a high cholesterol diet till sacrifice at the end of the experiment. The rabbits were euthanized in groups for histological evaluation after MRI examination at different time points of week 6 (n=6), week 12 (n=8) and week 15 (n=9), respectively.

MRI scan protocol

Serial MRI examinations were performed at the 6th, 12th and 15th week on a 1.5-T clinical MR system (Eclipse, Philips Medical Systems) with a standard knee coil. The rabbit was sedated with an intravenous injection of 40 mg/kg pentobarbital (Shanghai Chemical Reagent Co., Shanghai), allowing spontaneous respiration throughout the examination. MRI was performed with the rabbit being placed in a prone position. The applied MRI protocol was the following: TR/TE of 500/12.5 ms, FOV of 120×120 mm, Res of 384×256, spatial resolution of

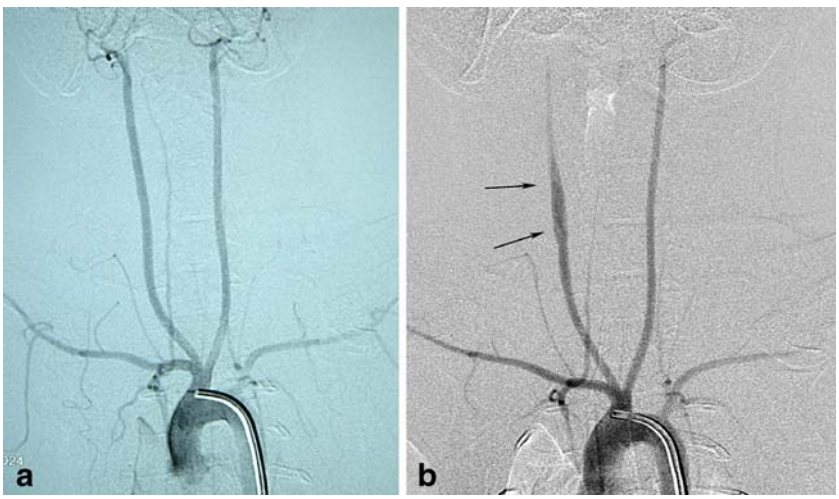

Fig. 1 Carotid arteriography before (**a**) and after (**b**) transcatheter balloon injury on the right common carotid artery (RCCA). Arrows indicate the injured RCCA with dilatation by a balloon catheter

0.312 mm, flip angle of 90°, slice thickness of 4.0 mm, and band width of 12.86 KHz with scan time of 6 min 40 s for T1-weighted imaging (T1WI) sequence; TR/TE of 3,000/68.4 ms, FOV of 120×120 mm, Res of 384×256, spatial resolution of 0.312 mm, flip angle of 90°, slice thickness of 4.0 mm, and band width 22.26 of KHz with scan time of 5 min 50 s for T2-weighted imaging (T2WI) sequence; and TR/TE of 3,000/15.0 ms, FOV of 120×120 mm, Res of 384×256, spatial resolution of 0.312 mm, flip angle of 90°, slice thickness of 4.0 mm and band width 25.26 KHz with scan time of 7 min 50 s for proton density-weighted imaging (PDWI) sequence.

Histopathological analysis

Immediately after sacrifice, the rabbit was perfusion-fixed with 10% formaldehyde, and the injured RCCA was excised. To facilitate this procedure and later co-localization between the MRI findings and histological specimen, the last MRI pictures were used as guidance taking the cervical vertebra as a land marker. The specimens were then embedded in paraffin and sectioned into slices of 4 μm in thickness for subsequent hematoxylin-eosin staining and microscopic observation.

Data analysis

The MR findings were interpreted independently by three radiologists (ZLM, GJT and XLM) who were experienced with vascular imaging, but blinded to the histological findings. Quantitative MRI analyses were also performed by them with consensus. The wall thickness of injured RCCA or the distance between the outer and inner borders of the cross section on the carotid artery was measured using commercial software (Neusoft PACS/RIS 3.0, Shenyang, China). The measurements were usually made on the PDW images, which typically yielded the highest contrast/noise (C/N) ratio, with T1W and T2W images cross-referenced. The per-slice mean values of the wall thickness from the adjacent five slices were averaged for each rabbit. In addition, atherosclerotic lesions were characterized in terms of lesion shape and type. The American Heart Association (AHA) classifications for atherosclerosis on MRI [9, 10] were employed for imaging analyses in this study. Briefly, type I and II denote nearly normal vessel wall thickness; type III refers to diffuse intimal thickening or small eccentric plaque with no calcification; type IV and V are plaques with a lipid or necrotic core surrounded by fibrous tissue with possible calcification; type VI is complex plaque with possible surface defect, hemorrhage or thrombus; type VII is a calcified plaque, and type VIII is fibrotic plaque without lipid core and with possible small calcification [9, 10].

The histopathological findings were independently interpreted and evaluated by three experienced pathologists (PSC, AFZ, ZYS) who were blinded to the MRI findings. All rabbits were measured histologically for the wall thickness of the RCCA by an image analysis software system (Motic Co, Xiamen, China). The values were averaged for the slices from five consecutive tissue blocks of the carotid arterial wall.

Atherosclerosis formation was histomorphologically evaluated according to the AHA classifications [11, 12]. Briefly, type I is the initial lesion with few foam cells, type II is fatty streaks with layers of multiple foam cells, type III is preatheroma with extracellular lipid pools, type IV is atheroma with a confluent extracellular lipid core, type V is fibroatheroma, type VI is complex plaque with possible surface defect, hemorrhage or thrombus, type VII is calcified plaque, and type VIII is fibrotic plaque without lipid core [11, 12]. Findings from cross-sectional histopathology were carefully compared with that from corresponding MRI.

Statistics

All obtained quantitative data were expressed as means ± standard deviation (SD). Statistical analyses were performed with the SPSS software (SPSS for Windows, version 11.0, 2001; SPSS, Chicago, IL). The agreement between the MR findings and the histological grades was statistically evaluated with Pearson coefficient correlation. P values<0.05 were considered statistically significant.

Results

MRI and histopathological findings in the 6th week Compared with the left uninjured carotid artery 6 weeks after balloon catheter intervention, the SI of injured RCCA was slightly higher on PDWI MRI (Fig. 2a). The MRI findings of the atherosclerosis formation in these rabbits could be classified as type I and type II based on the criteria of the AHA classifications. Histological examinations in these rabbits showed proliferation of intima and infiltration of inflammatory cells with abundant smooth muscle cells within the interstitium underneath the injured endothelium (Fig. 2b), which were conformable to the criteria for type I and II based on the AHA histological classifications and consistent with the corresponding MRI classifications (Table 1). The measured wall thickness of the RCCA was 0.2344±0.018 mm.

MRI and histopathological findings in the 12th week MRI in the 12th week showed that the injured arterial wall (0.513±0.032 mm) was thicker than that seen in the 6th week, and hyperintense on the T1WI and PDWI, but

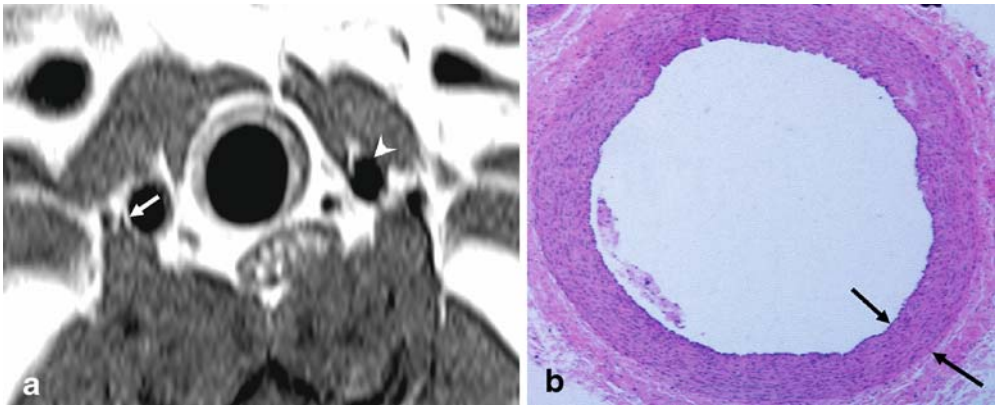

Fig. 2 In the 6th week after intervention on the rabbit, the axial section on proton density-weighted imaging (PDWI) showed the RCCA with a slightly increased signal intensity (SI) and arterial wall thickness (arrow) in comparison to the uninjured left carotid artery (arrowhead) (**a**). Corresponding histological section of the RCCA showed that the intima (confronting arrows) of the injured arterial wall was mainly composed of proliferated smooth muscle cells (**b**) (HE staining, ×40)

hypointense on the T2WI (Fig. 3a–c). The carotid wall thickness as measured histologically was 0.305±0.024 mm, which was comparable to that derived from MRI if 60–70% of shrinkage due to dehydration during histological preparations was taken into account. Based on the criteria of the AHA classifications for MRI evaluation, of eight rabbits in this group, two were classified as type II and six as type III, whereas the histopathological classifications of these rabbits showed one as type I, five as type III and two as type IV (Table 1). On histomorphology, the plaques at this stage were mainly characterized by enriched foam cells and smooth muscle cells (Fig. 3d).

MRI and histological findings in the 15th week MRI in the remaining rabbits in the 15th week showed much more thickened vessel wall (0.659±0.058 mm) with narrowing lumen in the injured RCCA (Fig. 4a–c). Of nine rabbits, two were recognized as type III, five as type IV and two as type V based on the AHA classifications for MRI. Histopathological findings corresponded well to that from MRI with the wall thickness of the RCCA measured as 0.48±0.041 mm. The plaques at this stage were primarily composed of smooth muscle cells, foam cells and soft lipid-rich core (Fig. 4d). AHA classifications showed one rabbit as type III, five as type IV and three as type V (Table 1).

Correspondence between MRI and histopathological findings The measured wall thickness on MRI correlated well with the morphometric histology as supported by the correlation coefficients of r=0.86 (P=0.006) at the 12th week and r=0.69 (P=0.043) at the 15th week, respectively. The lipid components of the vessel wall were showed as hyperintense regions both on T_1WI and PDWI (Fig. 4a,b) and hypointense on T_2WI (Fig. 4c). According to the eight types in the AHA classifications for both MRI and histolopathological findings, in this study from the induced rabbit model, the consistency of type I and II between MRI and histology was 100% (6/6) in the 6th week. However, in the 12th week the identification of type III dropped to 75.0% and 62.5% on MRI and histopathology, respectively. In the 15th week, the identification of type IV and type V was 55.6% and 22.2% on MRI, and 55.6% and 33.3% on histology, respectively. The agreement between MRI and histopathology for atherosclerosis classification was statistically significant (p=0.0368) as evaluated with Person correlation test (Table 2).

Table 1 MRI versus histopathological classifications of atherosclerosis

Types	I, II	III	IV	V	VI	VII	VIII
6 weeks (n=6)	6(6)*						
12 weeks (n=8)	2(1)*	6(5)*	(2)*				
15 weeks (n=9)		2(1)*	5(5)*	2(3)*			

( )* The numbers of animals on histolopathological classifications

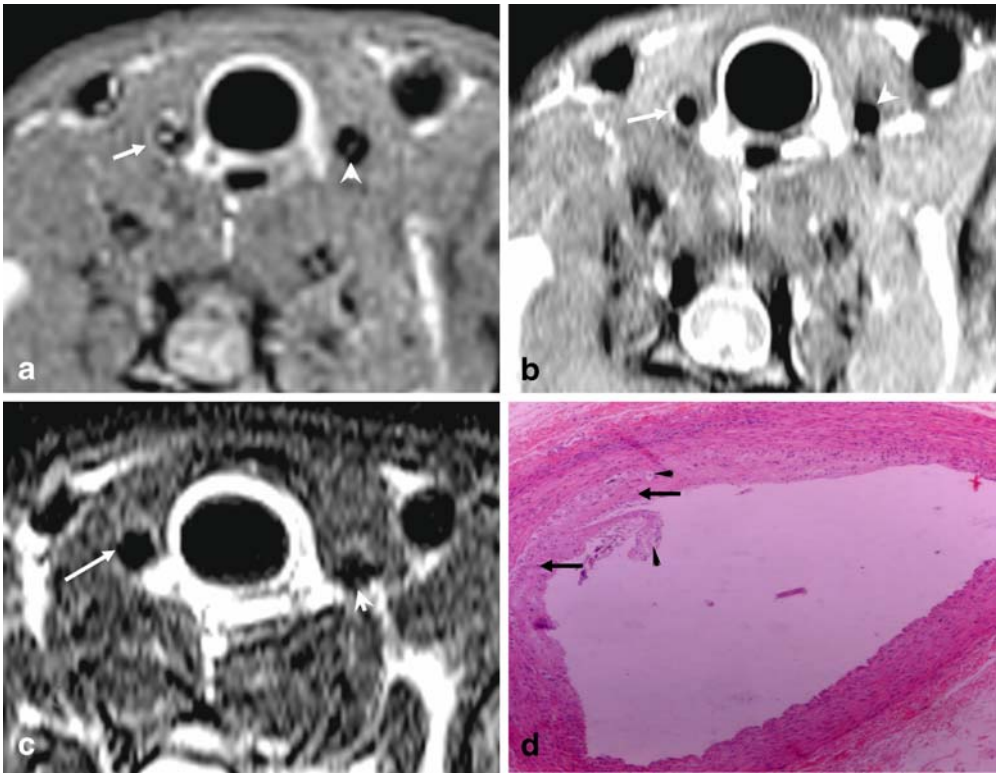

Fig. 3 In the 12th week, MRI showed that relative to the uninjured left carotid artery (arrowhead), the injured RCCA wall (arrow) became thicker with higher SI on T1WI (**a**) and PDWI (**b**), but appeared hypointense on T_2WI (**c**). The histological examination (**d**) demonstrated that the atherosclerotic plaque was composed of foam cells (arrows) and the smooth muscle cells (arrowheads) (HE staining, ×40)

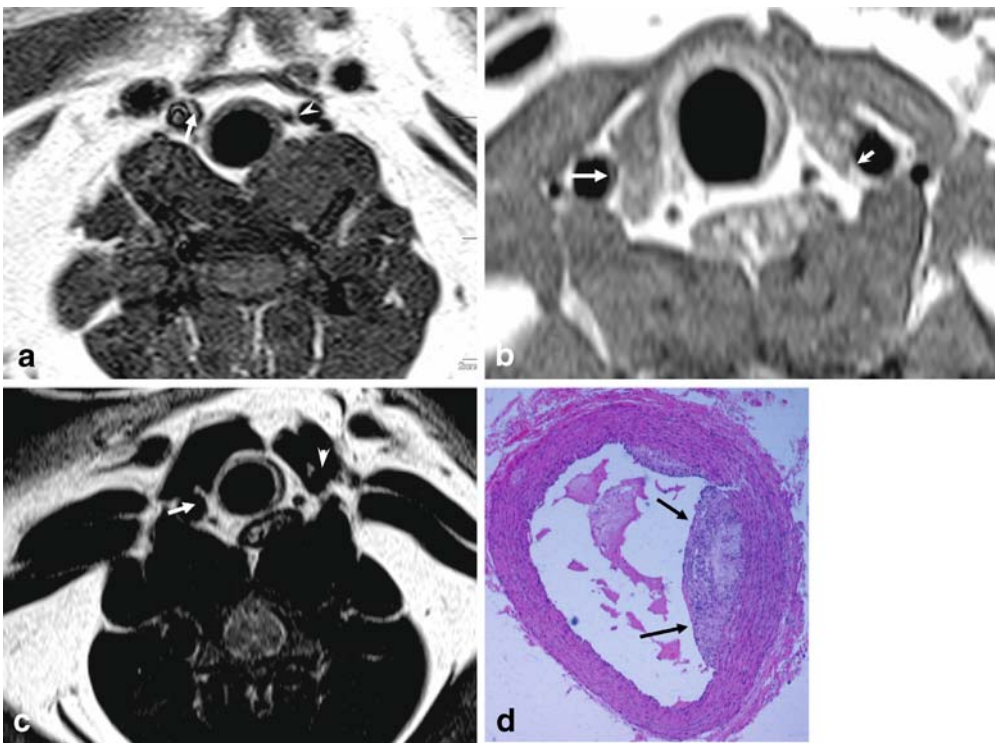

Fig. 4 In the 15th week, MRI showed that relative to the uninjured left carotid artery (arrowhead), the injured RCCA wall (arrow) contained greater plaque with hyperintensity on T_1WI (**a**) and PDWI (**b**), but appeared hypointense on T_2WI (**c**). Histological section (**d**) corresponding to (**a**–**c**) showed larger and more extensive plaques (arrows) with a significantly narrower lumen of the injured artery (HE staining, ×40)

Table 2 Correlationship between MRI and histopathological classification positive rate of atherosclerosis

Types	I, II	III	IV	V	VI	VII	VIII
Positive rate of MR	100%(6/6)	75.0%(6/8)	55.6%(5/9)	22.2%(2/9)			
Positive rate of histology	100%(6/6)	62.5%(5/8)	55.6%(5/9)	33.3%(3/9)			

Correlation test: Pearson correlation coefficient (r=0.96), p=0.0368

Discussion

The histopathological changes of atherosclerosis take place in vessel wall and can be generally classified as the following three categories: fatty streak, fibrous plaque and complicated lesions [3, 9, 10]. Conventional imaging techniques such as angiography are optimized only to detect the focal and high-grade stenosis without the ability to identify vessel wall changes, since the arteries can compensate for the progressive growth of atherosclerotic plaques by increasing their external circumference, thereby maintaining lumen diameter [13]. Therefore, the radiological assessment of atherosclerosis needs to shift emphasis from the vascular lumen to the arterial wall. The extravascular ultrasound, which is routinely used to evaluate the carotid arteries, is still largely based on location and degree of stenosis and limited in its ability to distinguish lipid-rich from collagenous layers within plaques. Therefore, this technique cannot generate any specific information for atherosclerotic plaque formation [14, 15]. Intravascular ultrasound (IVUS) can delineate the thickness and echogenicity of vessel wall structures; however, IVUS is limited in detection of thrombus and lipid-rich lesions, and it is an intrinsically invasive modality [16]. On the other hand, MRI is advantageous over other existing techniques. It has the ability similar to that of IVUS to accurately evaluate the vessel wall area without invasive maneuvers; unlike X-ray based angiography, it does not involve ionizing radiation or arterial catheterization; with the best intrinsic soft tissue contrast and ever-improving spatial resolution, it provides images of both the vessel wall and lumen, and it can be repeatedly applied for serial follow-up studies [17]. An additional advantage of MRI is that it may offer the possibility to allow co-registration of both molecular and anatomical information within a single imaging mode [18, 19]. Therefore, MRI may become the leading noninvasive in vivo imaging modality for the assessment of atherosclerotic burden.

MRI studies on atherosclerosis in various animal models, including rabbits [17], have been widely reported [20, 21]. Atherosclerosis of the aorta is the most frequent model used for MRI investigations, and few studies were involved in carotid artery in rabbit models [13]. The reasons why we selected the RCCA of rabbits for our experiments are the following: (1) carotid artery atherosclerosis refers to one of the highest clinical prevalence of the disease; (2) anatomically common carotid artery of relatively large size is located in a superficial position with a straight course and insignificant motion, all of which make it highly suitable for MRI evaluation of the vessel wall using a surface coil or a cylindrical knee coil; (3) the symmetric presence of the contralateral left common carotid artery serves as a perfect intraindividual control artery for MRI comparative analyses.

The appearances of atherosclerosis formation in rabbit as shown on MRI in this study are similar to those as reported by the other researchers, e.g., lipid components of the vessel wall as hyperintense regions both on T_1WI and PDWI, but hypointense on T_2WI [22].

The correlation between MRI and pathological findings of atherosclerotic formation process in rabbit models has been investigated by other authors [23, 24]. However, they mainly focused on the relationship between measurements of vessel wall thickness with MRI and histopathology. There were few studies that paid attention to the correlation between MRI classifications and histopathological classifications of the atherosclerosis in rabbit models. The present study not only showed a good correlation of the wall thickness as measured with MRI and morphometric histology, but also demonstrated that the histopathological process of atherosclerosis formation can be monitored by using a 1.5-T clinical MRI scanner. Furthermore, advancement of atherosclerosis from type I to type V in this particular rabbit model combining RCCA injury and lipid diet during the 15 weeks of observation is evident with both MRI and pathological findings. Therefore, MRI may be a useful investiagtion to show the particular types of atherosclerosis both in rabbit models and human patients.

There are several limitations in this study. Firstly, advanced stages of type VI to VIII of atherosclerosis were encountered in neither histopathology nor MRI in this series over 15 weeks, which calls for further investigations. Secondly, similar to other studies [25, 26], lack of the features of human atheroma makes the rabbit model difficult for the study of atherosclerosis progressing toward plaque vulnerability and rupture, which is important in the clinical situations. Thirdly, since dedicated phased-array radiofrequency coils or state-of-the-art clinical MRI scanners were not available at the time of this study, the delicate imaging quality in differentiating fibrous from

lipid components of the atherosclerotic lesions in our study with this rabbit model appears not as good as that of the others with high-resolution imaging systems [27].

In summary, the present study suggested that using a 1.5-T clinical MRI scanner should be feasible to visualize atheroma burden and types of atherosclerotic formation in a rabbit model of carotid arterial atherosclerosis. Such a study should be of great help to the laboratory research on pathogenesis, diagnosis and treatment of atherosclerosis.

Acknowledgement This research project was partially supported by the National Natural Science Foundation of China 90606007 and an award by the Hwa Ying Education and Culture Foundation 2007.

References

1. Yach D, Hawkes C, Gould CL, Hofman KJ (2004) The global burden of chronic diseases: overcoming impediments to prevention and control. JAMA 291:2616–2622
2. Duvall WL, Vorchheimer DA (2004) Multi-bed vascular disease and atherothrombosis: scope of the problem. J Thromb Thrombolysis 17:51–61
3. Cullen P, Rauterberg J, Lorkowski S (2005) The pathogenesis of atherosclerosis. Handb Exp Pharmacol 170:3–70
4. Goldschmidt-Clermont PJ, Creager MA, Lorsordo DW, Lam JK, Wassef M, Dzau VJ (2005) Atherosclerosis: 2005 recent discoveries and novel hypotheses. Circulation 112:3348–3353
5. Chu B, Phan BA, Balu N, Yuan C, Brown BG, Zhao XQ (2006) Reproducibility of carotid atherosclerotic lesion type characterization using high resolution multicontrast weighted cardiovascular magnetic resonance. J Cardiovasc Magn Reson 8:793–799
6. Yuan C, Miller ZE, Cai J, Hatsukami T (2002) Carotid atherosclerotic wall imaging by MRI. Neuroimaging Clin N Am 12:391–401
7. Cai J, Hatsukami TS, Ferguson MS, Kerwin WS, Saam T, Chu B, Takaya N, Polissar NL, Yuan C (2005) In vivo quantitative measurement of intact fibrous cap and lipid-rich necrotic core size in atherosclerotic carotid plaque: comparison of high-resolution, contrast-enhanced magnetic resonance imaging and histology. Circulation 112:3437–3444
8. Babiarz LS, Astor B, Mohamed MA, Wasserman BA (2007) Comparison of gadolinium-enhanced cardiovascular magnetic resonance angiography with high-resolution black blood cardiovascular magnetic resonance for assessing carotid artery stenosis. J Cardiovasc Magn Reson 9:63–70
9. Leiner T, Gerretsen S, Botnar R, Lutgens E, Cappendijk V, Kooi E (2005) Magnetic resonance imaging of atherosclerosis. Eur Radiol 15(6):1087–1099
10. Cai JM, Hatsukami TS, Ferguson MS, Small R, Polissar NL, Yuan C (2002) Classification of human carotid atherosclerotic lesions with in vivo multicontrast magnetic resonance imaging. Circulation 106:1368–1373
11. Stary HC, Chandler AB, Glagov S, Guyton JR, Insull W Jr, Rosenfeld ME, Schaffer SA, Schwartz CJ, Wagner WD, Wissler RW (1994) A definition of initial, fatty streak, and intermediate lesions of atherosclerosis. A report from the Committee on Vascular Lesions of the Council on Arteriosclerosis, American Heart Association. Circulation 89:2462–3353
12. Stary HC, Chandler AB, Dinsmore RE, Fuster V, Glagov S, Insull W Jr, Rosenfeld ME, Schaffer SA, Schwartz CJ, Wagner WD, Wissler RW (1995) A definition of advanced types of atherosclerotic lesions and a histological classification of atherosclerosis. A report from the Committee on Vascular Lesions of the Council on Arteriosclerosis, American Heart Association. Circulation 92:1355–1374
13. Hegyi L, Hockings PD, Benson MG, Overend P, Grimsditch DC, Burton KJ, Lioyd H, Whelan GA, Skepper JN, Vidgeon-Hart MP, Carpenter AT, Reid DG, Suckling KE, Weissberg PL et al (2004) Short term arterial remodelling in the aorta of cholesterol fed New Zealand white rabbits shown in vivo by high-resolution magnetic resonance imaging - implications for human pathology. Pathol Oncol Res 10:159–165
14. Spence JD (2006) Technology Insight: ultrasound measurement of carotid plaque–patient management, genetic research, and therapy evaluation. Nat Clin Pract Neurol 2:611–619
15. Nighoghossian N, Derex L, Douek P (2005) The vulnerable carotid artery plaque: current imaging methods and new perspectives. Stroke 36:2764–2772
16. Brown BG, Zhao XQ (2007) Is intravascular ultrasound the gold standard surrogate for clinically relevant atherosclerosis progression? J Am Coll Cardiol 49:933–938
17. Manninen HI, Vanninen RL, Laitnen M, Rasanen H, Vainio P, Luoma JS, Pakkanen T, Tulla H, Yla-Herttuala S (1998) Intravascular ultrasound and magnetic resonance imaging in the assessment of atherosclerotic lesions in rabbit aorta: correlation to histopathologic findings. Invest Radiol 33:464–471
18. Briley-Saebo KC, Mulder WJ, Mani V, Hyafil F, Amirbekian V, Aguinaldo JG, Fisher EA, Fayad ZA (2007) Magnetic resonance imaging of vulnerable atherosclerotic plaques: current imaging strategies and molecular imaging probes. J Magn Reson Imaging 26:460–479
19. Jaffer FA, Libby P, Weissleder R (2007) Molecular imaging of cardiovascular disease. Circulation 116:1052–1–61
20. Wiesmann F, Szimtenings M, Frydrychowicz A, Illinger R, Hunecke A, Rommel E, Neubauer S, Haase A (2003) High-resolution MRI with cardiac and respiratory gating allows for accurate in vivo atherosclerotic plaque visualization in the murine aortic arch. Magn Reson Med 50:69–74
21. Chaabane L, Soulas EC, Contard F, Salah A, Guerrier D, Briguet A, Douek P (2003) High-resolution magnetic resonance imaging at 2 Tesla: potential for atherosclerotic lesions exploration in the apolipoprotein E knockout mouse. Invest Radiol 38:532–538
22. Kramer CM (2002) Magnetic resonance imaging to identify the high-risk plaque. Am J Cardiol 90:15L–17L

23. Wang YX, Kuribayashi H, Wagberg M, Holmes AP, Tessier JJ, Waterton JC (2006) Gradient echo MRI characterization of development of atherosclerosis in the abdominal aorta in Watanabe Heritable Hyperlipidemic rabbits. Cardiovasc Intervent Radiol 29:605–612
24. Hanni M, Edvardsson H, Wagberg M, Pettersson K, Smedby O (2004) Quantification of atherosclerosis with MRI and image processing in spontaneously hyperlipidemic rabbits. J Cardiovasc Magn Reson 6:675–684
25. McMahon AC, Kritharides L, Lowe HC (2005) Animal models of atherosclerosis progression: current concepts. Curr Drug Targets Cardiovasc Haematol Disord 5:433–440
26. Bengel FM (2006) Atherosclerosis imaging on the molecular level. J Nucl Cardiol 13:111–118
27. Yarnykh VL, Terashima M, Hayes CE, Shimakawa A, Takaya N, Nguyen PK, Brittain JH, McConnel MV, Yuan C (2006) Multicontrast black-blood MRI of carotid arteries: comparison between 1.5 and 3 Tesla magnetic field strengths. J Magn Reson Imaging 23:691–698